Biochimica et Biophysica Acta 1808 (2011) 307–315

Contents lists available at ScienceDirect

Biochimica et Biophysica Acta

journal homepage: www.elsevier.com/locate/bbamem

Correlated AFM and NanoSIMS imaging to probe cholesterol-induced changes in phase behavior and non-ideal mixing in ternary lipid membranes

Christopher R. Anderton [a], Kaiyan Lou [b], Peter K. Weber [c], Ian D. Hutcheon [c], Mary L. Kraft [b,*]

[a] Department of Chemistry, University of Illinois at Urbana-Champaign, Urbana, IL 61801, USA
[b] Department of Chemical and Biomolecular Engineering, University of Illinois at Urbana-Champaign, Urbana, IL 61801, USA
[c] Glenn Seaborg Institute, Lawrence Livermore National Laboratory, Livermore, CA 94551, USA

ARTICLE INFO

Article history:
Received 16 June 2010
Received in revised form 9 September 2010
Accepted 20 September 2010
Available online 29 September 2010

Keywords:
Secondary ion mass spectrometry
Atomic force microscopy
Lipid phase behavior
Cholesterol
Lipid composition
Phase separation

ABSTRACT

Cholesterol is believed to be an important component in compositionally distinct lipid domains in the cellular plasma membrane, which are referred to as lipid rafts. Insight into how cholesterol influences the interactions that contribute to plasma membrane organization can be acquired from model lipid membranes. Here we characterize the lipid mixing and phase behavior exhibited by ^{15}N-dilaurolyphosphatidycholine (^{15}N-DLPC)/deuterated distearoylphosphatiylcholine (D_{70}-DSPC) membranes with various amounts of cholesterol (0, 3, 7, 15 or 19 mol%) at room temperature. The microstructures and compositions of individual membrane domains were determined by imaging the same membrane locations with both atomic force microscopy (AFM) and high-resolution secondary ion mass spectrometry (SIMS) performed with a Cameca NanoSIMS 50. As the cholesterol composition increased from 0 to 19 mol%, the circular ordered domains became more elongated, and the amount of ^{15}N-DLPC in the gel-phase domains remained constant at 6–7 mol%. Individual and micron-sized clusters of nanoscopic domains enriched in D_{70}-DSPC were abundant in the 19 mol% cholesterol membrane. AFM imaging showed that these lipid domains had irregular borders, indicating that they were gel-phase domains, and not non-ideally mixed lipid clusters or nanoscopic liquid-ordered domains.

1. Introduction

Lateral variations in component distribution within the plasma membrane are required to coordinate membrane-mediated cellular functions [1–3]. The nonrandom distributions of certain proteins within the plasma membrane are well-established [4–9]. Lipids and cholesterol are also believed to be spatially organized in biological membranes, but whether their organization is driven by lipid–lipid or lipid–protein interactions is not clear [1–3]. In one model of plasma membrane organization, differential affinities between cholesterol and other membrane components are hypothesized to drive the formation of liquid-ordered, cholesterol- and sphingolipid-enriched nanoscale domains (diameters <300 nm) that are referred to as lipid rafts [1,3,10,11]. Thus, characterizing the effects of cholesterol-dependent interactions on component distribution within the plasma membrane is the goal of much research.

Insight into how lipid–cholesterol and lipid–lipid interactions might influence lipid organization within biological membranes has been acquired by studying model lipid membranes [12]. In the absence of cholesterol, membranes composed of a low and high melting temperature lipid component homogeneously mix when heated above the melting transition temperature (T_m) of both lipid species, but separate into disordered fluid-phase and ordered gel-phase domains when cooled below the T_m of the high-melting temperature lipid species [13,14]. The addition of cholesterol to the membrane affects the lipid miscibility and domain microstructure observed at room temperature in a manner that depends on the degree of saturation in the low-melting temperature lipid [15–18]. At low cholesterol concentrations, membranes composed of a di-unsaturated low T_m lipid, such as 1,2-dioleoyl-*sn*-glycero-3-phosphocholine (DOPC), and a high T_m lipid species exhibit macroscopic fluid- and gel-phase domains [14,15]. At higher cholesterol concentrations (mole fraction > ~0.16), the gel-phase is replaced by macroscopic liquid-ordered domains that coexist with the disordered fluid-phase [14,17–21]. Above a threshold cholesterol concentration (mole fraction > ~0.4), phase separation ceases and homogeneous lipid mixing occurs [14,17–21]. In contrast, macroscopic liquid-ordered domains are usually not detected in cholesterol-containing ternary membranes in which the lipid species with the low T_m is saturated, such as 1,2-dilauroyl-*sn*-glycero-3-phosphocholine (DLPC) [14,15,17,18,22–25]. The gel-phase domains that coexist with the disordered fluid-phase

Abbreviations: FRET, fluorescence resonance energy transfer; AFM, atomic force microscopy; SIMS, secondary ion mass spectrometry; ^{15}N-DLPC, ^{15}N-1,2-dilauryl-*sn*-glycero-3-phosphocholine; D_{70}-DSPC, 1,2-distearoyl-D_{70}-*sn*-glycero-3-phosphocholine; NBD-PC, 1-palmitoyl-2-{12-[(7-nitro-2-1,3-benzoxadiazol-4-yl)amino]lauroyl}-*sn*-glycero-3-phosphocholine; PC, phosphatidylcholine; GUVs, unilamellar vesicles, ROIs, regions of interest; T_m, melting transition temperature

* Corresponding author. Tel.: +1 217 333 2228.
E-mail address: mlkraft@illinois.edu (M.L. Kraft).

0005-2736/$ – see front matter © 2010 Elsevier B.V. All rights reserved.
doi:10.1016/j.bbamem.2010.09.016

undergo a reduction in size without the formation of macroscopic, liquid-ordered domains as the cholesterol concentration increases [15,22,23]. For example, Fig. 1 shows the ternary phase diagram determined by Zhao et al. for giant unilamellar vesicles composed of DLPC/1,2-distearoyl-*sn*-glycero-3-phosphocholine (DSPC)/cholesterol at room temperature [22]. At a threshold cholesterol concentration (0.15–0.2 mole fraction), phase separation could not be visualized in giant unilamellar vesicles (GUVs) using conventional fluorescence microscopy, but fluorescence resonance energy transfer (FRET) measurements indicate that the membrane is not homogeneously mixed [18,22]. This FRET behavior is postulated to be due to the presence of nanoscopic liquid-ordered domains in the membrane, even though tiny gel-phase domains and distinct lipid clusters transiently produced by non-ideal mixing may also be consistent with these results [18,20,22,25,26].

Although saturated, low T_m lipids are rarely found in cellular membranes, identification of how this change in lipid structure alters membrane phase behavior provides a better understanding of the physiological significance of fatty acid chain unsaturation in biological membranes. Moreover, demonstration of the existence of nanoscopic liquid-ordered domains in model lipid membranes would indicate that lipid–lipid and lipid–cholesterol interactions are sufficient to produce liquid-ordered domains with dimensions similar to those that may exist in biological membranes. Despite the significance of such a finding, whether the nanoscale heterogeneity detected in membranes composed of DLPC, DSPC, and a threshold cholesterol concentration is due to the presence of liquid-ordered domains, gel-phase domains, or non-ideally mixed transient lipid assemblages has not been definitively established.

A key difference between phase-separated domains and non-ideally mixed transient lipid clusters is that the composition and microstructure would be constant between nanoscopic phase-separated domains of the same phase, as opposed to varying from one structure to another in non-ideally mixed lipid assemblages [18]. Liquid-ordered and gel-phase domains can be discriminated by their microstructures, as the edges of liquid-ordered domains are smooth and rounded, whereas the perimeters of gel-phase domains are angular and jagged [18,22,23,27]. The membrane thickness may also differ between gel-phase and liquid-ordered domains [28]. Therefore, information on the composition and microstructure of individual domains is required to identify whether the lipid structures detected at the threshold cholesterol concentration are non-ideally mixed lipid assemblages or phase-separated domains in the gel- or liquid-ordered phase. The microstructure, and therefore phase, of submicron-sized lipid assemblages within supported lipid bilayers can be characterized with atomic force microscopy (AFM) even when the domain sizes are below the lateral resolution of conventional fluorescence microscopy [15,16,23,25,29,30].

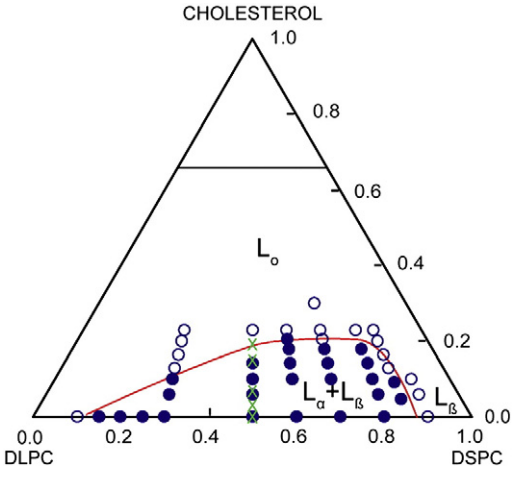

Fig. 1. Ternary phase diagram for giant unilamellar vesicles composed of DLPC/DSPC/cholesterol at room temperature. Uniform fluorescence and phase separation was observed at compositions marked by "○" and "●", respectively. Green crosses "X" mark the compositions of the vesicles used to form the supported lipid membranes that were characterized with AFM and NanoSIMS in this study (an equal molar ratio of DLPC/DSPC with 0, 3, 7, 15, and 19 mol% cholesterol). Reprinted from Ref. [22] with permission from Elsevier. Phase notation for liquid-ordered (L_o), gel (L_β) phase and fluid (L_α) phase from Gosku and Longo [47] have been added.

Assessing the lipid composition of individual lipid domains is more challenging because few analytical techniques yield spatially resolved and chemically specific information. Secondary ion mass spectrometry (SIMS) is one of the few approaches that enables imaging specific lipid species within supported lipid membranes with both chemical and spatial specificity [30–40]. Time-of-flight SIMS (TOF-SIMS) is a molecular imaging approach that has the advantage of not requiring labels for lipid identification, but the lateral resolution and sensitivity is seldom sufficient to characterize submicron-sized lipid domains [41]. Recently, a combination of high-resolution SIMS performed with a Cameca NanoSIMS 50 and lipid-specific isotope labeling has permitted the distributions of two isotopically labeled lipid species in phase-separated supported lipid membranes to be imaged with 100-nm-lateral resolution and quantified [31], rendering this a promising approach to analyze the lipid composition within nanoscopic lipid domains (diameters <300 nm). The Cameca NanoSIMS 50 is a magnetic sector mass spectrometer that can image differences in elemental and isotopic composition [42]. To identify and image different lipids using a NanoSIMS, each lipid species must contain a distinct stable isotope so that the secondary ions generated during analysis can be linked to the parent lipid species [42].

Here we use AFM and NanoSIMS to characterize the effects of cholesterol addition on the microstructure and composition of lipid domains in ternary membranes composed of the saturated, low T_m lipid ^{15}N-1,2-dilauryl-*sn*-glycero-3-phosphocholine (^{15}N-DLPC), and the high T_m lipid 1,2-distearoyl-D_{70}-*sn*-glycero-3-phosphocholine (D_{70}-DSPC). We investigated the cholesterol concentrations between 0 and 19 mol%. Over this range of cholesterol concentrations, GUVs composed of DLPC/DSPC exhibit macroscopic phase-separated domains and nanoscale heterogeneous mixing that is postulated to signify the presence of tiny liquid-ordered domains [18,22]. Supported lipid membranes are the subject of these studies to permit analyses with NanoSIMS and AFM. Although discrepancies in the phase behavior of supported membranes and GUVs have been reported [25], we avoided the non-equilibrium effects potentially induced by the solid support by using slow-cooled vesicle fusion to prepare the supported membranes, as demonstrated by Longo and co-workers [23]. Analysis of the same regions of the membrane with both AFM and NanoSIMS enabled correlation of domain microstructure with lipid composition, and allowed us to assess whether the nanoscopic lipid assemblages that occur near the threshold cholesterol concentration are non-ideally mixed clusters, or phase-separated lipid domains in either a gel or liquid-ordered state. As shown later, the AFM and NanoSIMS data indicate that the nanoscopic lipid assemblies within the 19 mol% cholesterol membrane are gel-phase domains.

2. Materials and methods

2.1. Materials

The chrome-patterned, oxidized silicon substrates (10-nm-thick oxide layer) were prepared as previously described [31] using silicon wafers that were a generous gift from Prof. Steven G. Boxer (Stanford University, Stanford CA). The lipids 1-palmitoyl-2-{12-[(7-nitro-2-1,3-benzoxadiazol-4-yl)amino]lauroyl}-*sn*-glycero-3-phosphocholine (NBD-PC) and 1,2-distearoyl-D_{70}-*sn*-glycero-3-phosphocholine (D_{70}-DPSC) were purchased from Avanti Polar Lipids, Inc (Alabaster, AL), and ^{15}N-1,2-dilauryl-*sn*-glycero-3-phosphocholine (^{15}N-DLPC)

was synthesized as reported [31]. To minimize possible oxidation, cholesterol was freshly synthesized from i-cholesteryl methyl ether (Sigma) as reported [43]. The cholesterol and phospholipid concentrations in the vesicle solutions were measured with the Amplex® Red Cholesterol Assay Kit and the Amplex® Red Phospholiase D Assay Kit, respectively, from Molecular Probes (Eugene, OR). Millipore (18 mΩ) water was used in all experiments.

2.2. Preparation of supported lipid membranes

Small unilamellar vesicles were created from an equal molar ratio of ^{15}N-DLPC ($T_m = -1$ °C) to D_{70}-DPSC ($T_m = 50.5$ °C [44]), and approximately 0, 2.5, 5, 10, 15, 20, or 35 mol% cholesterol. The actual cholesterol concentrations in the final vesicle solutions measured with enzymatic assays (Section 2.3) were 0, 3, 7, 15, 19, 27, and 35 mol%. A small amount (1 mol%) of the fluorescent lipid, NBD-PC, was added to the mixture to allow the evaluation of membrane integrity and the presence of phase separation using fluorescence microscopy. These components were dissolved in chloroform, dried under nitrogen, and placed under a vacuum to remove residual chloroform. The lipid film was resuspended in 65 °C water to a final lipid concentration of 0.5 mg/mL. The lipid solution was heated in a 65 °C water bath for 15 min, vortexed, transferred to a plastic tube, and sonicated using a tip sonicator (Branson Tip Sonifier Model 250, Branson Ultrasonics, Danbury CT) for 30 s intervals until it became transparent. The vesicle solution was reheated to 65 °C in a water bath, and 2.5 mL of 65 °C vesicle solution was added to a 60-mm-diameter × 15-mm-tall polystyrene culture dish containing multiple chrome-patterned, oxidized silicon substrates submerged in 2.5 mL of 65 °C water. The culture dish was covered, incubated at room temperature for 40 min to allow for bilayer formation, and then was transferred into a 65 °C water bath. The substrates were gently shaken under water to dislodge vesicles adhered to the bilayer's surface, and were transferred to a fresh 65 °C water bath. The water bath containing the substrates was placed in a programmable oven (ECHOterm™ IN35 Programmable Chilling/Heating Incubator, Torrey Pines Scientific, San Diego, CA), maintained at 70 °C for 1 h, and then was slowly cooled to room temperature at a rate of 5 °C/h to induce phase separation. To prepare the lipid membranes for SIMS analysis, the samples were flash-frozen in liquid ethane and freeze-dried as previously described [31–33]. To evaluate sample quality, fluorescence imaging was performed on a Leica DM6000 B upright fluorescence microscope equipped with a fluorescence filter cube (GFP, Leica) that matches the excitation and emission spectra for NBD-PC.

2.3. Measurement of mol% cholesterol

The moles of cholesterol and phosphatidylcholine (PC) in each vesicle solution were measured using the Amplex® Red Cholesterol Assay Kit and the Amplex® Red Phospholiase D Assay Kit, respectively. The assays were performed in 96-well plates purchased from Costar® (Corning, NY), and the fluorescence intensity was read using a Synergy HT Multi-Mode Microplate Reader Model SIAFRT (Biotek® Instruments, Inc., Winooski, VT). Cholesterol and PC standards were used to create the calibration curves. Eight replicates were performed on each vesicle and standard solution. The μmole of cholesterol and PC measured in each small unilamellar vesicle solution was used to calculate the mol% of cholesterol. The mol% cholesterol in the supported lipid membranes is assumed to be the same as the cholesterol content in the vesicle solution used for bilayer formation.

2.4. AFM imaging of lipid membranes

AFM analysis was performed in ambient air and temperature using an Asylum MFP-3D™ Stand Alone AFM. AFM images were acquired of the phase-separated membranes within specific grid boxes, which were relocated and analyzed with the NanoSIMS. Measurements were taken with standard tapping 300 kHz AFM probes (Tap300Al-G, Budget Sensors, Bulgaria) in AC (tapping) mode operated in the repulsive tip-sample interaction regime to preserve tip lifetime. Images were flattened to the first order. The line scans were averaged over three pixels perpendicular to the line-section path to minimize random variations in height due to noise. The line scans made on the 19 mol% cholesterol membrane were not averaged because the domains were often smaller than the 3-pixel averaging width. For each cholesterol concentration investigated, the height difference between the gel- and fluid-phase regions was measured at ten different domain interfaces.

2.5. High-resolution SIMS analysis

SIMS was performed on a Cameca NanoSIMS 50 instrument (Cameca, France) at Lawrence Livermore National Laboratory (Livermore, CA). Measurements were made with a ~0.8 pA, 16 keV Cs^+ primary ion beam focused onto a ~100 nm-diameter spot with an analysis area of 25 μm × 25 μm. A beam diameter of 102 nm was determined using the reported knife-edge method [31]. Measurements consisted of six replicate scans of 512 × 512 pixels with a dwell time of 0.3 ms/pixel, and corresponded to a primary ion dose of ~3.8×10^{14} ions/cm^2. The analysis conditions used in this work were chosen to provide sufficient ion counts to characterize the samples while minimizing analysis time. Based on our analysis conditions, a total sputter time of 472 s, and the sputtering rate of 2.5 nm μm^2/pA s determined on other biological samples [45], we estimate that the sputtering depth was ~1.5 nm for these measurements. Based on the thickness of the bilayer, the analysis time could have been ~3 times longer, though the secondary ion intensities obtained in each additional replicate scan would be lower than the previous scan. The pixel size in the NanoSIMS ion images was 49 nm × 49 nm, which is smaller than the beam diameter. The secondary ion signals $^{12}C^-$, $^{12}CD^-$, and $^{12}C^{15}N^-$, and the secondary electron signal were collected simultaneously using multi-collection mode. A mass resolving power of ~7500 was used to separate isobaric interferences from the isotopes of interest, e.g., $^{12}C^2H$ from $^{13}C^1H$ and $^{12}C^1H_2$ at a nominal mass of 14 amu, and $^{12}C^{15}N$ from $^{13}C^{14}N$ at a nominal mass of 27 amu. Data were analyzed using a custom software package (L'image, L. Nittler, Carnegie Institution of Washington) run on the PV-Wave platform (Visual Numerics, Inc., Houston, TX). The lipid-specific ions ($^{12}CD^-$ and $^{12}C^{15}N^-$) were smoothed over 3 × 3 pixels (147 nm × 147 nm). Then the lipid-specific ion signal was normalized by dividing the intensity for each ion by the $^{12}C^-$ intensity measured at the same pixel in order to minimize random, concentration-independent changes in the signal intensity. Regions of interest (ROIs) on the calibration set of homogeneous lipid membranes were defined on areas of the substrate that were covered by the membrane, and excluded areas where the chrome grid or obvious defects were visible in the secondary electron image that was collected in parallel to the secondary ion images. ROIs on the phase-separated membranes that consisted of only gel-phase or fluid-phase regions were defined based on the correlated AFM images.

2.6. Determination of lipid composition within lipid phases

A calibration curve correlating the normalized $^{12}C^{15}N^-$ secondary ion intensity to the mol% ^{15}N-DLPC in the membrane was made as previously reported [31,32]. Briefly, NanoSIMS analysis was performed on homogeneous lipid bilayers that systematically varied in mol% ^{15}N-DLPC to unlabeled DLPC. These samples were used instead of ^{15}N-DLPC/cholesterol membranes in order to obtain a calibration curve that was accurate at both high and low ^{15}N-DLPC concentrations. The same analytical conditions were used for the calibration and phase-separated samples. We assessed the validity of these calibration

samples by calculating the relative sensitivity factors (RSF) [36] for the $^{12}C^{15}N^-$ using $^{12}C^-$ as the reference ion. For membranes composed of ^{15}N-DLPC/NBD-PC (99/1 mol%:mol%), ^{15}N-DLPC/cholesterol/NBD-PC (84/15/1 mol%/mol%/mol%), and ^{15}N-DLPC/cholesterol/NBD-PC (69/30/1 mol%/mol%/mol%), the RSF for $^{12}C^{15}N^-$ was 0.0089 ± 0.0003, 0.0093 ± 0.0017, and 0.0093 ± 0.0011, respectively. Note that these values are low because the intensity of the $^{12}C^-$ reference ion is very high. Because the RSF for $^{12}C^{15}N^-$ was ~4.5% higher in the presence of cholesterol, we expect that the mol% ^{15}N-DLPC that we calculate in membranes containing cholesterol may be overestimated by up to 5 mol%.

To create the calibration curve, the normalized $^{12}C^{15}N^-$ intensity ($^{12}C^{15}N^-/^{12}C^-$) was measured for several ROIs so that an area of at least 1000 μm^2 was analyzed on each homogeneous membrane sample of specified mol% ^{15}N-DLPC. The mean values and standard deviation of the normalized $^{12}C^{15}N^-$ signal were calculated for each mol% ^{15}N-DLPC. The normalized $^{12}C^{15}N^-$ intensity was plotted against the mol% ^{15}N-DLPC in the membrane (Fig. 2) where the error bars show one standard deviation, and the best-fit line for the calibration data was calculated by linear regression. For every cholesterol composition studied, the amount of ^{15}N-DLPC in the gel-phase was determined using the calibration curve to convert the normalized $^{12}C^{15}N^-$ intensity measured within gel-phase regions where trapped fluid-phase subdomains were not detected by AFM into mol% ^{15}N-DLPC. The normalized $^{12}C^{15}N^-$ intensity was measured at several ROIs on each sample, and the average mol% ^{15}N-DLPC in the gel-phase and standard deviation were calculated. Because NBD-PC is excluded from the gel-phase [31,46], the average amount of D_{70}-DSPC in the gel-phase regions of the cholesterol-free membrane was determined by subtracting the mol% ^{15}N-DLPC measured at membrane locations identified as gel-phase by AFM from 100 mol%.

3. Results

The cooling rate employed for bilayer formation determines whether the phase separation approaches equilibrium. All of the samples we studied were cooled to room temperature at the same rate to ensure that any variations in domain morphology were not due to differences in their thermal history. For compatibility with NanoSIMS analysis, the room temperature ^{15}N-DLPC/D_{70}-DSPC/cholesterol supported lipid membranes were flash-frozen and freeze-dried to remove the water without perturbing lipid organization [31]. Previous studies demonstrated that flash-freezing and freeze-drying do not induce further phase separation or other changes in membrane organization [31], and the preserved membrane structure reflects that present at room temperature prior to membrane preservation. The lipids in the membrane do not exhibit lateral mobility after freeze-drying, and the membrane organization does not change in the time between AFM imaging and NanoSIMS analysis (2–6 weeks). Note that the use of isotopically labeled lipids is not expected to alter membrane phase behavior because D_{70}-DSPC has nearly the same T_m as natural abundance DSPC (50.5 °C and 55.0 °C, respectively, [44]), and the single nitrogen-15 isotope in ^{15}N-DLPC should not affect its T_m.

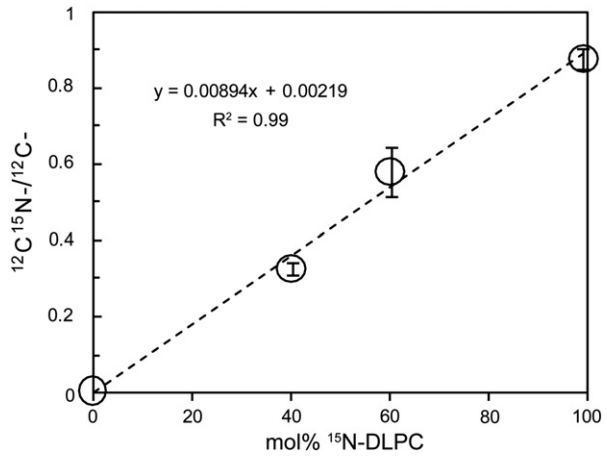

Fig. 2. Calibration curve correlating the normalized $^{12}C^{15}N^-$ ion intensity to the mol% ^{15}N-DLPC in the membrane, constructed by performing several NanoSIMS measurements on homogeneous lipid membranes of known mol% ^{15}N-DLPC. Error bars represent one standard deviation around the mean.

3.1. Cholesterol-free phase-separated supported lipid membranes

To correlate domain structure with lipid composition, we imaged the same locations within the phase-separated supported lipid membrane using both AFM and NanoSIMS. Similar to previous AFM studies of phase-separated supported lipid membranes [29–31,46,47], we observed circular gel-phase domains with a bimodal size distribution in the cholesterol-free membrane (Fig. 3 and supplemental images). Small gel-phase domains with diameters below 200 nm were primarily located near the perimeters of the large gel-phase structures that were several microns in diameter (Fig. 3a and b). Nanoscopic fluid-phase subdomains were also trapped inside of the micron-sized gel-phase domains. We measured a height difference of 1.3 nm at the interface between the gel- and fluid-phase domains (Fig. 3b, inset). This height difference is smaller than that previously reported between gel- and fluid-phase domains (1.8 nm) and is closer to the height difference between an asymmetric domain, with one gel-phase and one fluid-phase leaflet, and a symmetric fluid-phase domain [31,46]. However, NanoSIMS analysis of these domains (Fig. 3c and d) indicated they contain too little ^{15}N-DLPC to be asymmetric ^{15}N-DLPC/D_{70}-DSPC domains (see later). The smaller height difference we measured between the gel- and fluid-phases is likely due to our use of a repulsive tip-sample interaction for AFM imaging [48]. AFM imaging of similar samples performed with a repulsive tip-sample interaction yielded a height difference of 1.3 nm at the gel/fluid interface, but with a tip-sample interaction that fluctuated between repulsive and attractive, we measured a height difference of 1.6 nm at the same location (not shown), which is close to the 1.8 nm height difference that was previously reported [31,46].

NanoSIMS analysis was performed at the same membrane locations that were imaged with AFM. The normalized $^{12}CD^-$ ions (red) and $^{12}C^{15}N^-$ ions (green) were used to locate D_{70}-DSPC and ^{15}N-DLPC, respectively. The absence of lipid-specific ions at the some pixels is due to the low intensity of the minor isotopes, as the AFM image of the freeze-dried membrane does not show damage at these sites (Fig. 3a and b). Similar to previous reports, the area occupied by D_{70}-DSPC within the membrane appeared to be slightly lower than that expected based on the mol% D_{70}-DSPC in the vesicles used for membrane preparation [31]. This difference in the D_{70}-DSPC content within the supported membranes and the vesicles used for membrane formation is likely due to the selective adsorption of these different lipid species onto the substrate, or from a lipid exchange process [23,49].

Using the NanoSIMS calibration curves described earlier, we determined that the ^{15}N-DLPC concentration was ~97 mol% in the fluid-phase domains, and ~6 mol% in the gel-phase domains. Because NBD-PC is excluded from the gel-phase [31,46], the D_{70}-DSPC concentration in the gel-phase regions of the cholesterol-free membrane is ~94 mol%. These results are consistent with previous NanoSIMS studies of DLPC/DSPC membranes, and with phase diagram predictions that the gel-phase contains ≤10 mol% DLPC and the fluid-phase contains ≤10 mol% DSPC [31,50]. The one exception was at the edges of the large gel-phase domains, where the data occasionally suggest the fractions of D_{70}-DSPC and ^{15}N-DLPC within the same pixel

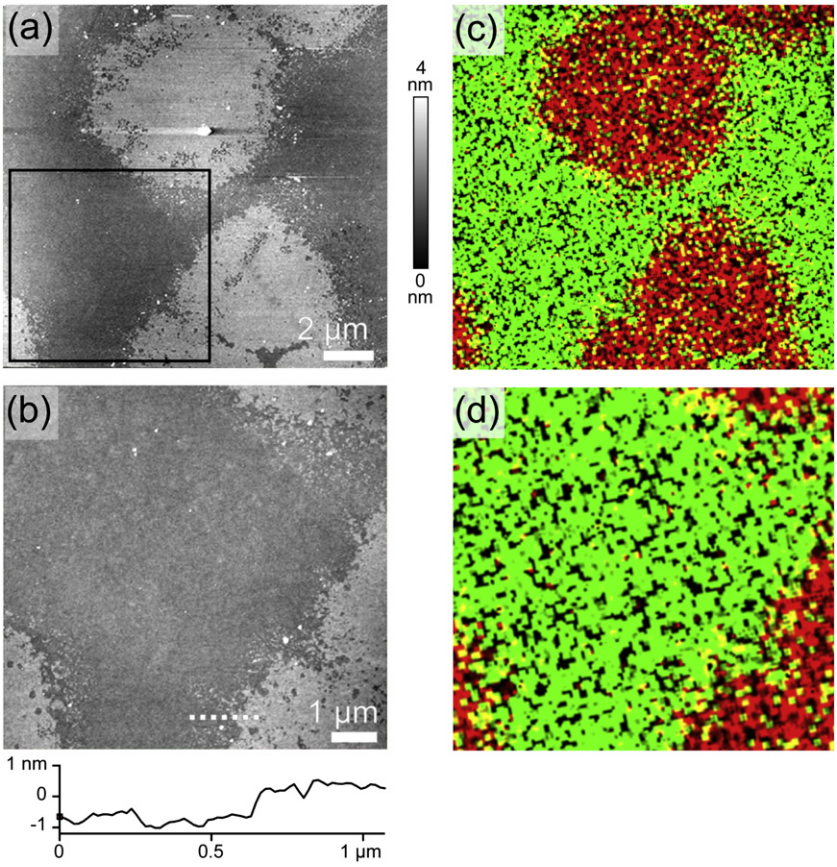

Fig. 3. AFM (a and b) and high-resolution SIMS images (c and d) of a phase-separated supported lipid membrane containing an equal molar ratio of D_{70}-DSPC and ^{15}N-DLPC without cholesterol. (a) AFM image shows gel- and fluid-phase membrane domains. (b) Higher resolution AFM image of the region outlined in (a). The line scan below the AFM image was acquired at the location indicated by the dashed line. (c) NanoSIMS images showing an overlay of the normalized ^{12}CD- (red) and ^{12}C^{15}N- (green) ion signals that localize D_{70}-DSPC and ^{15}N-DLPC, respectively, were acquired at the same site as the AFM image (a). The absence of lipid-specific ions at the regions that appear dark is due to the low intensity of the minor isotopes. (d) Detail of the region outlined in (a), which corresponds to the AFM image in (b). The NanoSIMS images were acquired with ~100-nm-lateral resolution and smoothed over a lateral resolution of ~150 nm.

(yellow areas, Fig. 3c and d) were more nearly equal. This might suggest that the amount of lipid mixing at the edges of the domains was greater than that predicted by phase-diagrams. However, the AFM images acquired at these sites show that the edges of the gel-phase domains are not smooth, but instead consist of many small crevices and peninsulas. Thus, the detection of elevated amounts of D_{70}-DSPC and ^{15}N-DLPC at the same pixel occurred because these structures were not resolved in these NanoSIMS images, which were acquired with a beam diameter of ~100 nm and were smoothed to the equivalent of ~150-nm-lateral resolution.

3.2. Phase-separated supported lipid membranes with 3–15 mol% cholesterol

The addition of cholesterol to the membrane induced an elongation of the macroscopic gel-phase domains. At 3 mol% cholesterol, the macroscopic D_{70}-DSPC-enriched gel-phase domains were oblong and had jagged borders (Fig. 4a and d, and supplemental images). A network of gel-phase domains was observed at 7 mol% cholesterol (Fig. 4b and e, and supplemental images). Similar to the cholesterol-free membrane, fluid-phase subdomains were entrapped within the macroscopic gel-phase structures, and gel-phase micro-domains were dispersed throughout the fluid-phase in the 3 and 7 mol% cholesterol membranes. A networked gel-phase structure that contained entrapped fluid-phase subdomains was also observed in the 15 mol% cholesterol membrane, but the edges of the gel-phase structures were smoother than those observed in the other membranes (Fig. 4c and f, and supplemental images). The area occupied by the D_{70}-DSPC-rich domains in the membranes that contained 7 and 15 mol% cholesterol was higher than that expected based on the compositions of the vesicles used for membrane formation. This difference in surface coverage was consistent across the membrane (see supplemental images). We attribute these results to the phenomena occurring during bilayer formation, such as the selective adsorption of the lipid species onto the substrate or lipid exchange, as opposed to selective incorporation of cholesterol into the ordered domains, because cholesterol is expected to evenly distribute between the two lipid phases [14]. Moreover, the increase in D_{70}-DSPC domain surface coverage seems larger than the fraction of cholesterol in the membrane. The height difference between the gel- and fluid-phase regions of the 3, 7, and 15 mol% cholesterol membranes did not change from that measured in the cholesterol-free membrane (~1.3 nm). Similarly, the ^{15}N-DLPC concentration within the D_{70}-DSPC-enriched domains remained constant at ~6 mol%, indicating that the solubility of ^{15}N-DLPC within the D_{70}-DSPC-rich domains did not change over this range of cholesterol concentrations. We did not attempt to quantify the mol% of ^{15}N-DLPC in the fluid-phase due to the high likelihood that the numerous nanoscopic gel-phase domains detected within the fluid-phase by AFM would inadvertently be included in the measurement.

3.3. Supported lipid membranes containing 19 mol% cholesterol and greater

Our AFM and NanoSIMS images of the 19 mol% cholesterol membrane clearly show heterogeneity in membrane composition

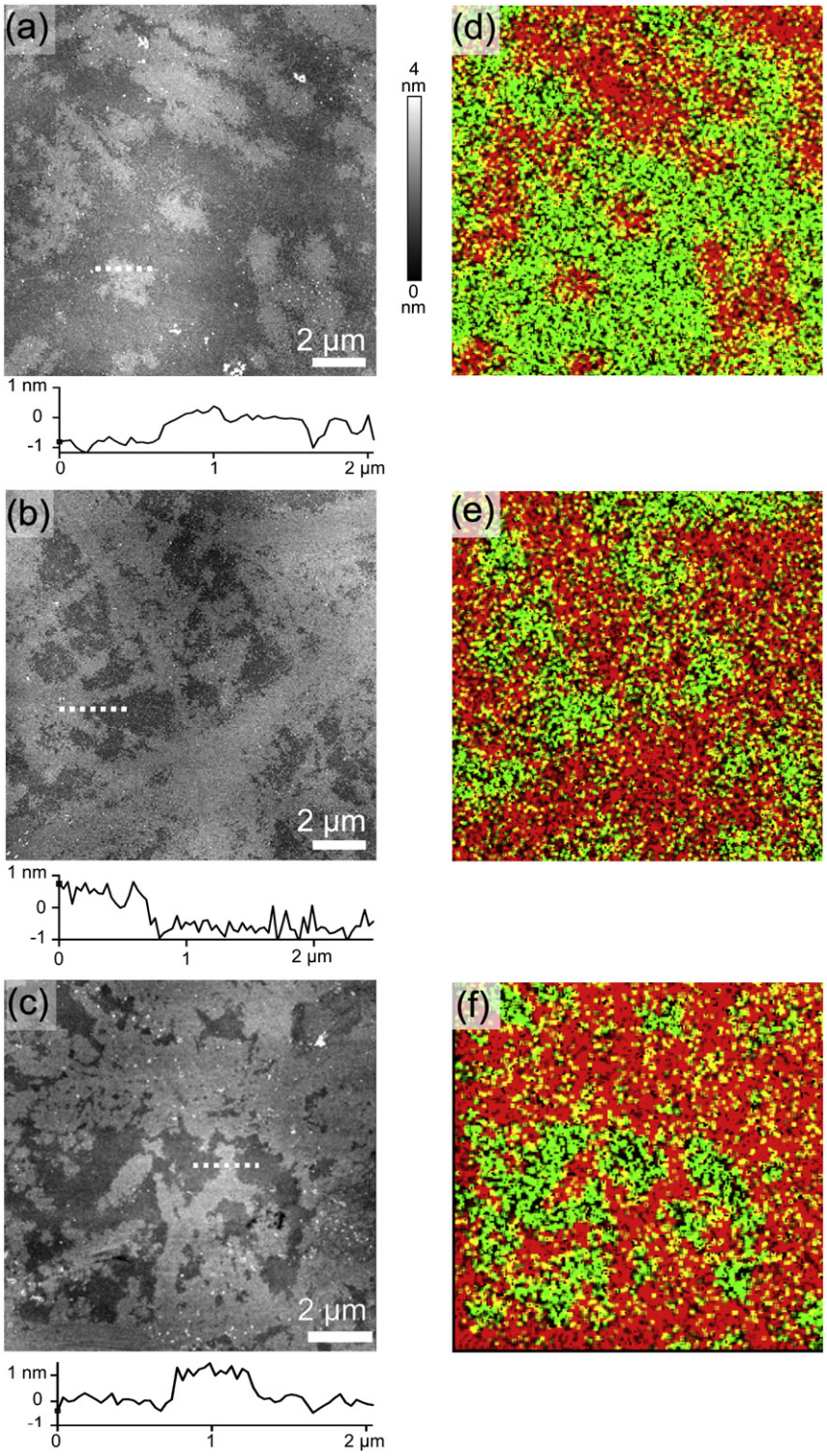

Fig. 4. AFM (a–c) and corresponding high-resolution SIMS (d–f) images of phase-separated membranes composed of a 1:1 molar ratio of D_{70}-DSPC to ^{15}N-DLPC, and 3 (a and d), 7 (b and e), and 15 mol% (c and f) cholesterol. The line scans below the AFM images were taken at the areas indicated by the dashed line.

and structure (Fig. 5). Individual and micron-sized aggregates of nanoscopic ordered domains enriched with D_{70}-DSPC are visible in the membrane. The height difference measured with AFM between the gel- and fluid-phases in the 19 mol% cholesterol membrane did not vary with domain size (~1.2 nm), and was similar to those measured in membranes with lower cholesterol levels (~1.3 nm). The ^{15}N-DLPC concentration within the submicron-size domains that were resolved in the NanoSIMS images was ~7 mol%, within one standard deviation of the value measured on the 0–15 mol% cholesterol membranes. Thus, a significant increase in lipid intermixing did not occur in these domains. However, elevated amounts of D_{70}-DSPC and ^{15}N-DLPC were detected at the same pixel more frequently in the 19 mol% cholesterol membrane than in the other membranes (yellow areas, Fig. 5d–f). Comparison to the AFM images acquired at these locations revealed the presence of nanoscopic lipid structures that were smaller than the resolution of the NanoSIMS

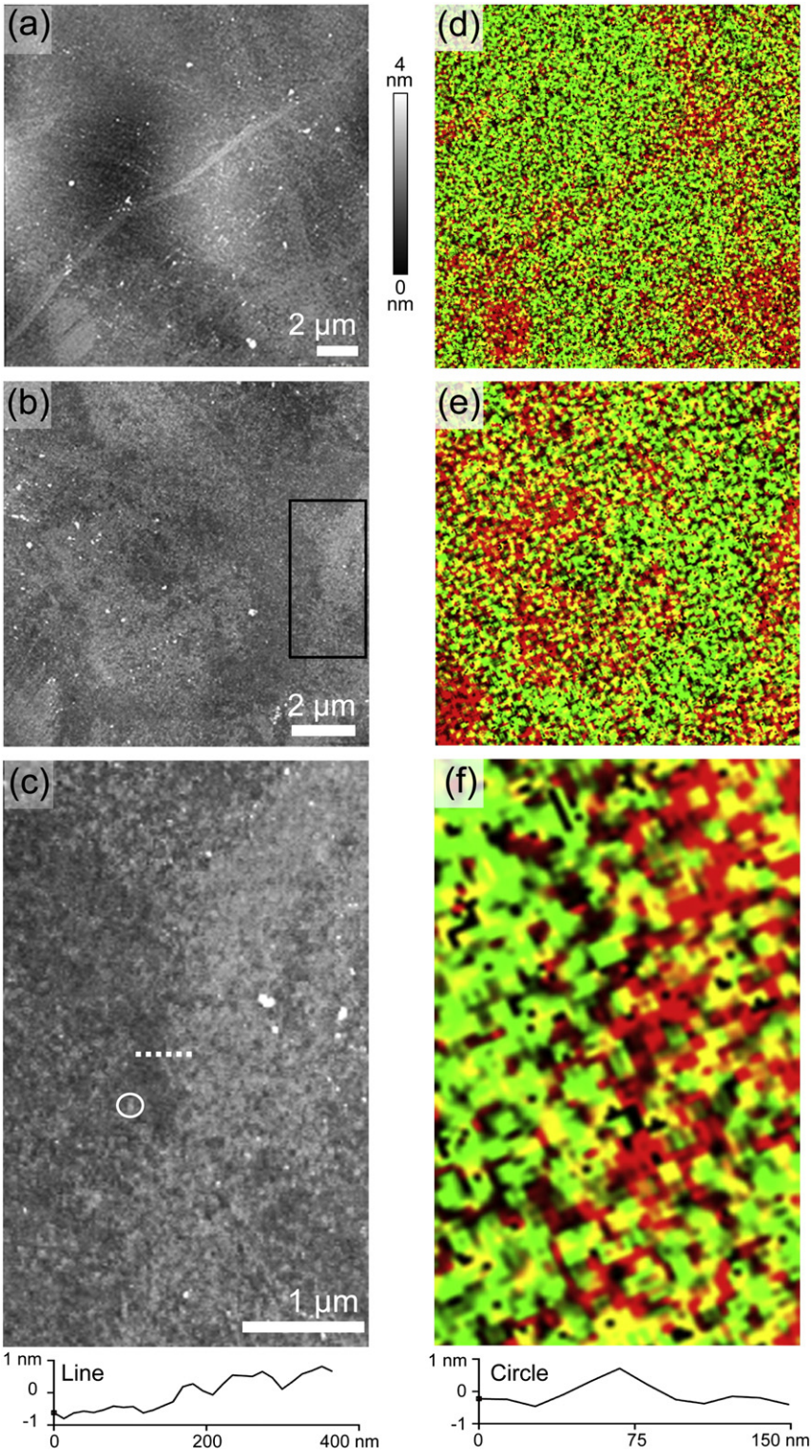

Fig. 5. AFM (a–c) and correlated high-resolution SIMS (d–f) images of a phase-separated membrane composed of a 1:1 molar ratio of D_{70}-DSPC to ^{15}N-DLPC and 19 mol% cholesterol. AFM images (a and b) of two different areas of the phase-separated membrane and corresponding SIMS images (d and e, respectively). (c) Higher resolution AFM scan of the area outlined with a rectangle in (b). The line scan below (c) was acquired at the edge of a cluster of nanoscopic domains, indicated by the dashed line in (c). The line scan below (f) was acquired at the nanoscopic lipid domain indicated by the circle in (c). (f) Enlarged SIMS image of the area indicated by the black rectangle in (b), which corresponds to the AFM image in (c).

images (Fig. 5a–c). Therefore, the detection of significant amounts of D_{70}-DSPC and ^{15}N-DLPC at the same pixel in the 19 mol% cholesterol membrane signifies the presence of a phase-separated domain that is smaller than the lateral resolution of the NanoSIMS image. The lack of an observable change in the height of the nanoscopic lipid structures or lipid intermixing denotes the presence of phase-separated domains, and not non-ideally mixed lipid clusters, in the 19 mol% cholesterol membrane. Because AFM imaging also shows that both

the micron-sized and nanoscopic lipid domains have irregular borders, we conclude that the domains enriched with D_{70}-DSPC remained in the gel-phase at 19 mol% cholesterol.

We also attempted to characterize supported lipid membranes that contained >19 mol% cholesterol (27 and 35 mol% cholesterol). These membranes exhibited numerous small height changes (<1 nm) and taller features indicative of debris by AFM, whereas patches of ^{15}N-DLPC and very little D_{70}-DSPC was detected on the substrate using the NanoSIMS (not shown). These features are not characteristic of those we have observed in poorly preserved membranes, nor do they resemble the dehydration-induced defects characterized by others [51]. These results suggest that high-quality supported lipid membranes did not form under the same conditions as those used to create the membranes with lower mol% cholesterol.

4. Discussion

4.1. Lipid organization in ^{15}N-DLPC/D_{70}-DSPC/cholesterol membranes

Using a combination of AFM and high-resolution SIMS to acquire correlated information on the structure and lipid distribution within ^{15}N-DLPC/D_{70}-DSPC/cholesterol membranes at room temperature, we found that the addition of up to 19 mol% cholesterol induced significant changes in domain morphology, but produced no observable change in the miscibility of ^{15}N-DLPC within the gel-phase. Unlike previous results in which the phase behavior of analogous supported membranes differed from that of GUVs [25], our results are in agreement with those reported for DLPC/DSPC/cholesterol GUVs and mica-supported membranes [22,47]. This good agreement indicates that the slow-cooled vesicle fusion process we employed for membrane formation likely allowed the membrane to approach equilibrium, and neither the silicon substrate nor the isotope labels appeared to alter membrane phase behavior.

According to the DLPC/DSPC/cholesterol phase diagram (Fig. 1), the miscibility point for a 1:1 molar ratio of DLPC/DSPC is ~19 mol% cholesterol, and non-ideal mixing postulated to be caused by nanoscopic liquid-ordered domains has been previously detected with FRET at slightly higher cholesterol concentrations (between 20 and 25 mol%) [18,22]. Yet gel-phase domains were present in our supported lipid membranes composed of DLPC/DSPC (1:1 molar ratio) and 19 mol% cholesterol. A higher amount of D_{70}-DSPC than ^{15}N-DLPC in the membrane, which could have occurred due to small gravimetric and volumetric errors in measuring the lipids, would shift the miscibility point to a higher cholesterol concentration (~20 mol%) than we studied [22]. However, we expect that nanoscopic gel-phase domains would also be present in our membranes at 20–21 mol% cholesterol because we detected a small number of micron-sized, gel-phase domains at 19 mol% cholesterol (Fig. 5a and b, lower left), and the gel-phase domains in supported lipid membranes undergo a reduction in size due to domain pinning before complete miscibility is reached [15,47]. This expectation is supported by a recent report by Gosku and Longo [47]. The speckling in Gosku and Longo's fluorescence microscopy images of mica-supported DLPC/DSPC/cholesterol (40/40/20 mol:mol:mol) membranes [47] suggests the presence of tiny phase-separated domains that could be detected by AFM, but were too small to be clearly visualized with fluorescence microscopy. We hypothesize that the small inconsistency in the location of the boundary for phase separation between our results and the published DLPC/DSPC/cholesterol phase diagram is due to the difference in techniques used to detect phase separation, as the AFM and NanoSIMS techniques we used are better suited to unambiguously detect submicron-sized domains than the conventional fluorescence microscopy [17,22,25,47].

The fusion of DLPC/DSPC (1:1 mol ratio) vesicles that contained 27 and 35 mol% cholesterol to the silicon substrates under conditions identical to those employed for the other cholesterol concentrations did not produce continuous, defect-free membranes. Increasing the cholesterol concentration within vesicles composed of phase-separating lipids is reported to hinder vesicle rupture, causing an increase in the critical number of vesicles that must adsorb to the silicon substrate in order to initiate vesicle fusion [52]. Because others have used vesicle fusion to form DLPC/DSPC (1/1 mole ratio) membranes that contained 30 mol% cholesterol on mica substrates [47], we hypothesize that the vesicle concentration or incubation time we employed for vesicle fusion was insufficient for the formation of defect-free membranes that contained 27 or 35 mol% cholesterol.

4.2. Significance and implications

Our data indicate that interactions between saturated lipids, such as DLPC and DSPC, and cholesterol are insufficient to drive the formation of liquid-ordered domains that are similar to those expected to exist within biological membranes. Our results, and those reported by others, suggest that molecular interactions between the fluid-phase lipid and cholesterol affect the structure of the ordered lipid domains that form in the membranes [15,23]. Although the DLPC/DSPC/cholesterol membranes we studied are not compositionally or biophysically representative of biological membranes, our findings do provide insight into the physiological significance of fatty acid chain saturation in biological membranes. Specifically, our results support the hypothesis that the presence of unsaturation in the fatty acid chains of the low-melting lipids found in biological membranes is required for the formation of a liquid-ordered phase. Furthermore, we propose that the absence of saturated, low T_m lipids in cellular membranes is functionally significant, as their presence may hinder the formation of liquid-ordered membrane domains.

This work also establishes a direct approach to acquire correlated information on the microstructure and composition of individual lipid domains. This approach could be extended to quantifying the amounts of DSPC and cholesterol in the lipid domains detected in these membranes by also incorporating a different distinct stable isotope into the cholesterol, and creating separate calibration curves for DSPC and cholesterol using sets of standard lipid membrane samples. Such studies would permit identifying whether the cholesterol concentration is equal in both lipid phases, as indicated by original experiments [14], or if the cholesterol concentration is higher in the ordered domains, as found for other lipid mixtures [18]. Our approach could also be used to construct more detailed phase-diagrams that include tie lines for DLPC/DSPC/cholesterol or other more physiologically relevant lipid mixtures. Such studies may clarify uncertainties in membrane phase behavior, and provide a better understanding of how cholesterol-dependent interactions contribute to cell membrane organization.

5. Conclusion

By analyzing the same locations in supported lipid membranes with AFM and high-resolution SIMS, we were able to acquire correlated information on the microstructure and composition of the individual lipid domains found in the membranes at room temperature. We showed that the nanoscopic D_{70}-DSPC domains present in the 19 mol% cholesterol membrane were in the gel-phase. The ^{15}N-DLPC concentration in the D_{70}-DSPC domains was relatively constant (6–7 mol%) for cholesterol concentrations between 0 and 19 mol%, indicating that cholesterol did not induce a significant increase in lipid intermixing in these domains. Our results support the finding of Zhao et al. [22] that nanoscopic phase-separated domains are present in the membrane at ~19 mol% cholesterol, but we found no evidence for the presence of liquid-ordered domains. We conclude that the interactions between cholesterol and saturated lipids, such as DLPC and DSPC, are not sufficient to create liquid-ordered domains. Consequently, the absence of saturated, low-melting lipids in

biological membranes may be required for the formation of the liquid-ordered domains that are expected to exist in cellular membranes.

Acknowledgements

We thank S. MacLaren for the helpful discussions on AFM, W. Hanafin for the assistance with the assays, S. Boxer for the oxidized silicon substrates, C. Ramon for the technical assistance, and L. Nittler for the software development. MLK holds a Career Award at the Scientific Interface from the Burroughs Wellcome Fund. Portions of this work were carried out in the Frederick Seitz Materials Research Laboratory Central Facilities, Univ. of Illinois, which are partially supported by the U.S. Department of Energy (DOE) under grants DE-FG02-07ER46453 and DE-FG02-07ER46471. Work at LLNL was supported by the Laboratory Directed Research and Development funding and performed under the auspices of the U.S. DOE under contract DE-AC52-07NA27344.

Appendix A. Supplementary data

Supplementary data to this article can be found online at doi:10.1016/j.bbamem.2010.09.016.

References

[1] J.F. Hancock, Lipid rafts: contentious only from simplistic standpoints, Nat. Rev. Mol. Cell Biol. 7 (2006) 456–462.
[2] A.S. Shaw, Lipid rafts: now you see them, now you don't, Nat. Immunol. 7 (2006) 1139–1142.
[3] D. Lingwood, K. Simons, Lipid rafts as an organizing principle, Science 327 (2010) 46–50.
[4] J. Omerovic, I.A. Prior, Compartmentalized signalling: Ras proteins and signalling nanoclusters, FEBS J. 276 (2009) 1817–1825.
[5] B.S. Wilson, J.R. Pfeiffer, J.M. Oliver, Observing FcER1 signaling from the inside of the mast cell membrane, J. Cell Biol. 149 (2000) 1131–1142.
[6] B.S. Wilson, S.L. Steinberg, K. Liederman, J.R. Pfeiffer, Z. Surviladze, J. Zhang, L.E. Samelson, L. Yang, P.G. Kotula, J.M. Oliver, Markers for detergent-resistant lipid rafts occupy distinct and dynamic domains in native membranes, Mol. Biol. Cell 15 (2004) 2570–2592.
[7] M. Takeda, G.P. Leser, C.J. Russell, R.A. Lamb, Influenza virus hemagglutinin concentrates in lipid raft microdomains for efficient viral fusion, Proc. Natl. Acad. Sci. U. S. A. 100 (2003) 14610–14617.
[8] S.T. Hess, T.J. Gould, M.V. Gudheti, S.A. Maas, K.D. Mills, J. Zimmerberg, Dynamic clustered distribution of hemagglutinin resolved at 40 nm in living cell membranes discriminates between raft theories, Proc. Natl. Acad. Sci. U. S. A. 104 (2007) 17370–17375.
[9] S.T. Hess, M. Kumar, A. Verma, J. Farrington, A. Kenworthy, J. Zimmerberg, Quantitative electron microscopy and fluorescence spectroscopy of the membrane distribution of influenza hemagglutinin, J. Cell Biol. 169 (2005) 965–976.
[10] K. Jacobson, O.G. Mouritsen, R.G.W. Anderson, Lipid rafts: at a crossroad between cell biology and physics, Nat. Cell Biol. 9 (2007) 7–14.
[11] L.J. Pike, The challenge of lipid rafts, J. Lipid Res. 50 (2009) S323–328.
[12] K. Simons, W.L.C. Vaz, Model systems, lipid rafts, and cell membranes, Annu. Rev. Biophys. Biomol. Struct. 33 (2004) 269–295.
[13] J.H. Ipsen, O.G. Mouritsen, Modeling the phase equilibria in two-component membranes of phospholipids with differing acyl-chain lengths, Biochim. Biophys. Acta 944 (1988) 121–134.
[14] G.W. Feigenson, Phase boundaries and biological membranes, Annu. Rev. Biophys. Biomol. Struct. 36 (2007) 63–77.
[15] W.C. Lin, C.D. Blanchette, M.L. Longo, Fluid-phase chain unsaturation controlling domain microstructure and phase in ternary lipid bilayers containing GalCer and cholesterol, Biophys. J. 92 (2007) 2831–2841.
[16] C.D. Blanchette, W.C. Lin, C.A. Orme, T.V. Ratto, M.L. Longo, Domain nucleation rates and interfacial line tensions in supported bilayers of ternary mixtures containing galactosylceramide, Biophys. J. 94 (2008) 2691–2697.
[17] D. Marsh, Cholesterol-induced fluid membrane domains: a compendium of lipid-raft ternary phase diagrams, Biochim. Biophys. Acta Biomembr. 1788 (2009) 2114–2123.
[18] G.W. Feigenson, Phase diagrams and lipid domains in multicomponent lipid bilayer mixtures, Biochim. Biophys. Acta 1788 (2009) 47–52.
[19] S.L. Veatch, S.L. Keller, Miscibility phase diagrams of giant vesicles containing sphingomyelin, Phys. Rev. Lett. 94 (2005) 148101–148104.
[20] S.L. Veatch, S.L. Keller, Seeing spots: complex phase behavior in simple membranes, Biochim. Biophys. Acta 1746 (2005) 172–185.
[21] S.L. Veatch, I.V. Polozov, K. Gawrisch, S.L. Keller, Liquid domains in vesicles investigated by NMR and fluorescence microscopy, Biophys. J. 86 (2004) 2910–2922.
[22] J. Zhao, J. Wu, H. Shao, F. Kong, N. Jain, G. Hunt, G.W. Feigenson, Phase studies of model biomembranes: macroscopic coexistence of Lα + Lβ with light-induced coexistence of Lα + Lo phases, Biochim. Biophys. Acta 1768 (2007) 2777–2786.
[23] C.D. Blanchette, W.C. Lin, T.V. Ratto, M.L. Longo, Galactosylceramide domain microstructure: impact of cholesterol and nucleation/growth conditions, Biophys. J. 90 (2006) 4466–4478.
[24] S.L. Veatch, S.L. Keller, Separation of liquid phases in giant vesicles of ternary mixtures of phospholipids and cholesterol, Biophys. J. 85 (2003) 3074–3083.
[25] F. Tokumasu, A.J. Jin, G.W. Feigenson, J.A. Dvorak, Nanoscopic lipid domain dynamics revealed by atomic force microscopy, Biophys. J. 84 (2003) 2609–2618.
[26] G.W. Feigenson, J.T. Bulboltz, Ternary phase diagram of dipalmitoyl-PC/dilauroyl-PC/cholesterol: nanoscopic domain formation driven by cholesterol, Biophys. J. 80 (2001) 2775–2788.
[27] A.V. Samsonov, I. Mihalyov, F.S. Cohen, Characterization of cholesterol-sphingomyelin domains and their dynamics in bilayer membranes, Biophys. J. 81 (2001) 1486–1500.
[28] P.E. Milhiet, M.-C. Giocondi, C. Le Grimellec, Cholesterol is not crucial for the existence of microdomains in kidney brush-border membrane models, J. Biol. Chem. 277 (2002) 875–878.
[29] L.J. Johnston, Nanoscale imaging of domains in supported lipid membranes, Langmuir 23 (2007) 5886–5895.
[30] J. Popov, D. Vobornik, O. Coban, E. Keating, D. Miller, J. Francis, N.O. Petersen, L.J. Johnston, Chemical mapping of ceramide distribution in sphingomyelin-rich domains in monolayers, Langmuir 24 (2008) 13502–13508.
[31] M.L. Kraft, P.K. Weber, M.L. Longo, I.D. Hutcheon, S.G. Boxer, Phase separation of lipid membranes analyzed with high-resolution secondary ion mass spectrometry, Science 313 (2006) 1948–1951.
[32] M.L. Kraft, S.F. Fishel, C. Galli Marxer, P.K. Weber, I.D. Hutcheon, S.G. Boxer, Quantitative analysis of supported membrane composition using the NanoSIMS, Appl. Surf. Sci. 252 (2006) 6950–6956.
[33] C. Galli Marxer, M.L. Kraft, P.K. Weber, I.D. Hutcheon, S.G. Boxer, Supported membrane composition analysis by secondary ion mass spectrometry with high lateral resolution, Biophys. J. 88 (2005) 2965–2975.
[34] J. Björn, ToF-SIMS imaging of lipids in cell membranes, Surf. Interface Anal. 38 (2006) 1401–1412.
[35] C.M. McQuaw, A.G. Sostarecz, L. Zheng, A.G. Ewing, N. Winograd, Lateral heterogeneity of dipalmitoylphosphatidylethanolamine-cholesterol Langmuir–Blodgett films investigated with imaging mass spectrometry and atomic force microscopy, Langmuir 21 (2005) 807–813.
[36] C.M. McQuaw, L. Zheng, A.G. Ewing, N. Winograd, Localization of sphingomyelin in cholesterol domains by imaging mass spectrometry, Langmuir 23 (2007) 5645–5650.
[37] P.D. Piehowski, A.J. Carado, M.E. Kurczy, S.G. Ostrowski, M.L. Heien, N. Winograd, A.G. Ewing, MS/MS methodology to improve subcellular mapping of cholesterol using TOF-SIMS, Anal. Chem. 80 (2008) 8662–8667.
[38] P.D. Piehowski, A.M. Davey, M.E. Kurczy, E.D. Sheets, N. Winograd, A.G. Ewing, M.L. Heien, Time-of-flight secondary ion mass spectrometry imaging of subcellular lipid heterogeneity: Poisson counting and spatial resolution, Anal. Chem. 81 (2009) 5593–5602.
[39] P.D. Piehowski, M.E. Kurczy, D. Willingham, S. Parry, M.L. Heien, N. Winograd, A.G. Ewing, Freeze-etching and vapor matrix deposition for ToF-SIMS imaging of single cells, Langmuir 24 (2008) 7906–7911.
[40] M.C. Biesinger, D.J. Miller, R.R. Harbottle, F. Possmayer, N.S. McIntyre, N.O. Petersen, Imaging lipid distributions in model monolayers by ToF-SIMS with selectively deuterated components and principal components analysis, Appl. Surf. Sci. 252 (2006) 6957–6965.
[41] P. Williams, Biological imaging using secondary ions, J. Biol. 5 (2006) 18.
[42] S.G. Boxer, M.L. Kraft, P.K. Weber, Advances in imaging secondary ion mass spectrometry for biological samples, Annu. Rev. Biophys. 38 (2009) 53–74.
[43] H. McKennis Jr., The formation of cholesterol from i-cholesteryl methyl ester, J. Biol. Chem. 172 (1948) 313–316.
[44] D. Guard-Friar, C.H. Chen, A.S. Engle, Deuterium isotope effect on the stability of molecules: phospholipids, J. Phys. Chem. 89 (1985) 1810–1813.
[45] S. Ghosal, S.J. Fallon, T.J. Leighton, K.E. Wheeler, M.J. Kristo, I.D. Hutcheon, P.K. Weber, Imaging and 3D elemental characterization of intact bacterial spores by high-resolution secondary ion mass spectrometry, Anal. Chem. 80 (2008) 5986–5992.
[46] W.C. Lin, C.D. Blanchette, T.V. Ratto, M.L. Longo, Lipid asymmetry in DLPC/DSPC-supported lipid bilayers: a combined AFM and fluorescence microscopy study, Biophys. J. 90 (2006) 228–237.
[47] E.I. Goksu, M.L. Longo, Ternary lipid bilayers containing cholesterol in a high curvature silica xerogel environment, Langmuir 26 (2010) 8614–8624.
[48] J. Schneider, Y.F. Dufrêne, W.R. Barger Jr., G.U. Lee, Atomic force microscope image contrast mechanisms on supported lipid bilayers, Biophys. J. 79 (2000) 1107–1118.
[49] A. Wikstrom, S. Svedhem, M. Sivignon, B. Kasemo, Real-time QCM-D monitoring of electrostatically driven lipid transfer between two lipid bilayer membranes, J. Phys. Chem. B 112 (2008) 14069–14074.
[50] S. Mabrey, J.M. Sturtevant, Investigation of phase transitions of lipids and lipid mixtures by high sensitivity differential scanning calorimetry, Proc. Natl. Acad. Sci. U. S. A. 73 (1976) 3862–3866.
[51] S.V. Bennun, R. Faller, M.L. Longo, Drying and rehydration of DLPC/DSPC symmetric and asymmetric supported lipid bilayers: a combined AFM and fluorescence microscopy study, Langmuir 24 (2008) 10371–10381.
[52] M. Sundh, S. Svedhem, D.S. Sutherland, Influence of phase separating lipids on supported lipid bilayer formation at SiO_2 surfaces, Phys. Chem. Chem. Phys. 12 (2010) 453–460.